Published OnlineFirst August 3, 2010; DOI: 10.1158/1535-7163.MCT-09-1147

Preclinical Development

Molecular Cancer Therapeutics

Overexpression of GRIM-19 in Cancer Cells Suppresses STAT3-Mediated Signal Transduction and Cancer Growth

Takashi Okamoto, Takashi Inozume, Hiroshi Mitsui, Mirei Kanzaki, Kazutoshi Harada, Naotaka Shibagaki, and Shinji Shimada

Abstract

Constitutive activation of signal transducer and activator of transcription 3 (STAT3) is common in many human and murine cancer cells, and its activation leads to cellular transformation. STAT3 pathway inhibitors have been reported to suppress cancer growth. To investigate the antitumor effects of inhibiting the STAT3-mediated signaling cascade in the cancer microenvironment, using a molecular-targeting approach, we focused on the gene associated with retinoid-IFN-induced mortality 19 (GRIM-19). GRIM-19 has been reported to interact physically with STAT3 and inhibit STAT3-dependent signal transduction. We used the nona-arginine (R9)-protein transduction domain (R9-PTD) as a protein carrier to induce high levels of GRIM-19 expression *in vitro* and *in vivo*. We generated an R9-PTD–containing GRIM-19 fusion protein (rR9-GRIM19) and successfully induced overexpression in the cytoplasm of cancer cells. Analysis of the expression of downstream molecules of STAT3 confirmed that *in vitro* rR9-GRIM19 treatment of constitutively activated STAT3 (STAT3c) cancer cells significantly reduced STAT3-dependent transcription. Moreover, intratumoral injections of rR9-GRIM19 in STAT3c cancer-bearing mice significantly suppressed tumor growth. These results suggest that intratumoral injections of rR9-GRIM19 have potential as a novel anticancer therapy in STAT3c cancer due to their ability to inhibit STAT3-mediated signal transduction without major systemic side effects. *Mol Cancer Ther; 9(8); 2333–43. ©2010 AACR.*

Introduction

Signal transducer and activator of transcription 3 (STAT3) belongs to the STAT family of latent, cytosolic transcription factors that directly relay signals from the plasma membrane to the nucleus (1). This protein is constitutively activated (phosphorylated) by aberrant upstream tyrosine kinase activities in a broad spectrum of human and murine tumors (1). Previous studies have shown that constitutive activation of STAT3 is associated with transformation by viral sarcoma (v-Src) and other oncoproteins that activate tyrosine kinase signaling pathways (2, 3). Moreover, constitutively activated STAT3 mutants directly induce cellular transformation, leading to unrestricted cell proliferation, antiapoptosis, and angiogenesis (4). Recently, immunosuppression associated with constitutively activated STAT3 has been reported in several tumor models (5–7). Therefore, the development of pharmacologic inhibitors of STAT signaling has potential in the treatment of human cancers. Several approaches addressing this issue have been reported, including blocking ligand-receptor interaction; inhibiting receptor and non-receptor tyrosine kinase; activating phosphotyrosine STAT3 phosphatases; and blocking STAT3 dimerization, nuclear translation, DNA binding, and gene transcription (8–10). Antisense gene therapy and RNA interference approaches have also been attempted (11).

The gene associated with retinoid-interferon–induced mortality 19 (GRIM-19) was originally identified by screening for interferon-β (IFN-β)– and retinoic acid–induced cell death in mammary carcinoma cells (12). GRIM-19 is expressed in normal tissues such as the adult heart, muscle, liver, kidney, placenta, spleen, and bone marrow (12). GRIM-19 codes for a novel 16 kDa protein, which is present in the cytoplasm and nucleus of the cells and also in the mitochondrion (13–15). The expression of GRIM-19 is upregulated by stimulating IFN-β and retinoic acid. Loss or downregulation of GRIM-19 in cancer cells has also been reported (16). Recently, some reports have shown that GRIM-19 directly binds to STAT3 but not to other STAT family members. Moreover, GRIM-19 inhibits STAT3-dependent gene transcription by interfering with DNA binding (17, 18). Transfection of GRIM-19 cDNA into cell lines in which STAT3 is constitutively activated downregulated the expression of downstream molecules of STAT3 and reduced cell growth (12, 16,

Authors' Affiliation: Department of Dermatology, Faculty of Medicine, University of Yamanashi, Yamanashi, Japan

Note: Supplementary material for this article is available at Molecular Cancer Therapeutics Online (http://mct.aacrjournals.org/).

Corresponding Author: Naotaka Shibagaki, University of Yamanashi, 1110 Shimokato, Chuo, Yamanashi 409-3898, Japan. Phone: 81-55-273-9856; Fax: 81-55-273-6766. E-mail: naotakas@yamanashi.ac.jp

doi: 10.1158/1535-7163.MCT-09-1147

Published OnlineFirst August 3, 2010; DOI: 10.1158/1535-7163.MCT-09-1147

19, 20). Therefore, we focused on this molecule as an appropriate candidate for molecular cancer therapy.

We have shown that protein transduction domain (PTD)–containing fusion proteins, particularly nona-arginine (R9)-PTD, were efficient and safe protein carriers (~100%) for any type of cell *in vitro* and *in vivo* (21–24). PTDs are incorporated into cells through macropinocytosis/endocytosis after binding to anionic cell membrane components such as heparan sulfate (25–27). It has been suggested that PTDs leak into the cytoplasm after macropinocytosis (25, 26). Recently, we reported that R9-PTD–containing proteins were localized at the site of injection area for a long time when injected i.d. and transduced into local tissue cells, including cancer mass (23). Thus, R9-PTD–containing fusion proteins offer a unique therapeutic opportunity for the treatment of many diseases.

In the present study, we have succeeded in expressing a significant amount of GRIM-19 protein in culture and *in vivo* using the R9-PTD–containing GRIM-19 fusion protein (rR9-GRIM19). Our results clearly indicate that rR9-GRIM19–treated STAT3-activated cancer cells, but not STAT3-inactivated cells, effectively suppressed STAT3-mediated signal transduction and cell growth.

Materials and Methods

Mice and cells

Female BALB/c and C57BL/6 mice (ages 6–8 weeks) were purchased from SLC Japan (Hamamatsu, Japan). All animal experiments were approved by the institutional review board of the University of Yamanashi Faculty of Medicine. Murine malignant melanoma cells, B16; murine B-cell lymphoma cells, A20; murine thymoma cells, EL-4; and murine fibroblasts, NIH3T3 were purchased from the American Type Culture Collection. EL-4 with OVA cDNA stable-transfectant cells EG.7 were provided by M. Bevan (University of Washington, Seattle, WA). NIH3T3 with v-Src cDNA stable-transfectant, v-Src NIH3T3 cells were provided by T. Iwamoto (Chubu University, Aichi, Japan). Cell lines were cultivated in RPMI 1640 containing 10% fetal bovine serum, glutamine, and penicillin/streptomycin (Invitrogen Japan).

Generation and characterization of recombinant proteins

His_6-tagged recombinant nona-arginine-hemagglutinin-ovalbumin (rR9-HA-OVA), rHA-GFP, rR9-HA-GFP, and rR9-HA-murine Fc receptor-like A (mFCRL) constructs were generated as previously described (21–23). *Leishmania* homologue of receptors for activated C kinase (LACK), known as highly immunogenic foreign antigen in *Leishmania major* (28), cDNA was provided by D. Sacks (National Institute of Allergy and Infectious Disease, Bethesda, MD). Constructs encoding His_6-tagged R9-HA-LACK were generated by inserting LACK cDNA (+427 to +939, 170 amino acids) in-frame into multiple cloning sites (*Nco*I/*Eco*RI) of the pR9-HA plasmid. Similarly, R9-HA-GRIM19 was generated by inserting full-length GRIM19 cDNA (derived from the murine heart tissues with GRIM19-specific primers containing enzyme recognition sites) in-frame into the pR9-HA plasmid. rR9-fusion proteins were purified as described previously (22).

Analysis of R9-PTD–mediated green fluorescent protein transduction in live cells

For the evaluation of green fluorescent protein (GFP) transduction, NIH3T3, A20, B16, and EG.7 cells were incubated with rHA-GFP or rR9-HA-GFP (600 nmol/L) as described (23).

Evaluation of the efficiency of GRIM-19 protein transduction in cell lines

NIH3T3, A20, B16, and EG.7 cells were incubated with rR9-GRIM19 (600 nmol/L for 6 hours), washed twice, fixed with 4% paraformaldehyde, and permeabilized with 0.2% NP40. After blocking with 5% goat serum, cells were incubated with 1 mg/mL anti-HA monoclonal antibody (Covance) or 1 mg/mL isotype IgG (Jackson ImmunoResearch Laboratories) as a primary antibody, followed by incubation with Cy-3–conjugated anti-mouse IgG (Jackson ImmunoResearch Laboratories) as the secondary antibody. Stained cells were analyzed using fluorescence microscopy/laser scanning confocal microscopy (Leitz DMRBF and Leica TCS4D; Leica).

Western blotting analysis

Anti–phospho-STAT3, anti–Bcl-xl (Tyr705; Cell Signaling Technology), anti–actin-R, anti-STAT3, anti–Bcl-2 (Santa Cruz Biotechnology), and anti–GRIM-19 (Calbiochem) antibodies were used as primary antibodies. Cells were collected and lysed. Total lysates (20 μg) were electrophoresed on a 4% to 12% Bis-Tris gel (Invitrogen Japan), and then transferred to a nitrocellulose membrane. After blocking the membrane with 3% bovine serum albumin in PBS containing 0.1% Tween 20, the membrane was incubated with the primary antibody overnight, washed three times with PBS containing 0.1% Tween 20 (10 minutes each time), incubated with the horseradish peroxidase–conjugated secondary antibody (IgG) for 1 hour, and washed four times with PBS containing 0.1% Tween 20. The signal was visualized with the SuperSignal West Dura Extended Duration Substrate (Thermo Fisher Scientific, Inc.).

Luciferase reporter assay

For the luciferase assay, v-Src NIH3T3 and NIH3T3 cells were transiently transfected using the TransFast transfection reagent (Promega) with luciferase plasmids containing the STAT3-binding enhancer sequence (hSIE; CATTTCCCGTAAATC) upstream of the cytomegalovirus promoter site of the control pGL-3 promoter plasmid (pGL hSIE) and the control pGL-3 promoter plasmid without any enhancer sequences (pGL promoter; Promega) in 12-well plates. The *Renilla* reporter construct pRL-TK plasmid (Promega) was also used to normalize the transfection efficiency. The cells were incubated for 24 hours in RPMI

Published OnlineFirst August 3, 2010; DOI: 10.1158/1535-7163.MCT-09-1147

1640 containing 10% fetal bovine serum, then treated with rR9-GRIM19 or the rR9-control protein (rR9-LACK) for 24 hours. Cells were washed with PBS and lysed with 100 μL of passive lysis buffer (Promega). Luciferase activity was determined using the Dual-Luciferase Reporter Assay System (Promega).

Quantitative real-time PCR

The relative expression of cyclin B1 and Bcl-xl (downstream molecules of STAT3) mRNA between cells treated with rR9-GRIM19 and the rR9-control (rR9-LACK) for 24 hours was determined by real-time PCR using the ABI Prism 5500 Sequence Detection System (PE Biosystems) with SYBR Green I dye (Qiagen), according to the manufacturer's instructions. Primers corresponding to cyclin B1, Bcl-xl, and glyceraldehyde 3-phosphate dehydrogenase (GAPDH) were designed as follows: 5′-CTAAGCACCAGATCAGACAG-3′ and 5′-CATGAGGTATTTGGCCAAAG-3′ for cyclin B1 (149 bp), 5′-GTGGAAAGCGTAGACAAGGA-3′ and 5′-GTTCCCGTAGAGATCCACAA-3′ for Bcl-xl (153 bp), and 5′-CGTGTTCCTACCCCCAATGT-3′ and 5′-TGTCATACTTGGCAGGTTTCT-3′ for GAPDH (126 bp). Cycle threshold numbers (Ct) were derived from the exponential phase of PCR amplification. Fold differences in the expression of gene × in cell population *y* and *z* were derived by 2^k, where $k = (Ctx - Ct_{GAPDH})y - (Ctx - Ct_{GAPDH})z$.

Electrophoretic mobility shift assay

Nuclear extracts were isolated from cultured cells using a nuclear and cytoplasmic extraction reagent (Pierce). Nuclear extracts were assayed for DNA binding to biotin-labeled, double-stranded oligonucleotides containing the STAT3 hSIE binding site (5′-CATTTCCCGTAAATC-3′; Operon Biotechnologies). Electrophoretic mobility shift assay (EMSA) was done using the Lightshift Chemiluminescent EMSA kit (Pierce). Biotin-labeled oligonucleotides (20 fmol) were incubated with nuclear proteins (10 μg) for 20 minutes at room temperature in a binding buffer [10 mmol/L Tris (pH 7.5), 50 ng/μL poly (dI-dC), 0.05% NP40, 5 mmol/L $MgCl_2$, and 2.5% glycerol]. Binding was hampered by 20-fold excess unlabeled hSIE oligonucleotides (cold), anti-STAT3 antibody (Santa Cruz C-20; sc-482X), and R9-fusion protein. These were incubated for 20 minutes after incubation of the nuclear proteins with the biotin-labeled oligonucleotides. STAT3-hSIE complexes were resolved by electrophoresis using a 6% DNA Retardation Gel (Invitrogen Japan), transferred to Biodyne B precut modified nylon membranes (Pierce), UV cross-linked, and visualized using the Chemiluminescent Nucleic Acid Detection system (Pierce).

Pull-down and Western blotting analyses

To confirm the direct interactions between rR9-GRIM19 and STAT3, pull-down assay was done using Profound Pull-Down PolyHis Protein:Protein Interaction Kit (Thermo Fisher Scientific, Inc.), according to the manufacturer's instruction. Briefly, purified polyhistidine-tagged bait proteins (rR9-GRIM19 and rR9-LACK) were immobilized to cobalt chelate affinity resin column. Prey proteins from v-Src NIH3T3 cell lysate were captured by applying to the column. Bait-prey elution was prepared with 290 mmol/L imidazole elution buffer. Electrophoresis samples (interacting proteins) were visualized by SDS-PAGE and Western blotting analyses with anti-STAT3 antibody.

Cell growth assay

Cells were plated in six-well plates in triplicate in the presence of the AG490 (Jak2/gp130 inhibitor, which works well as a STAT3 inhibitor; Alexis Biochemicals) or rR9-fusion protein [600 (nmol/L)/mL/well]. Cell number was counted at 48 and 96 hours.

Propidium iodide–Annexin assay

A20 and EG.7 cells (1×10^6) were grown in six-well plates and treated with PBS, rR9-control (rR9-LACK), rR9-GRIM19, and AG490 for 48 hours. Cells were stained using the Annexin V-FLUOS Staining Kit (Roche), according to the manufacturer's protocol. Cells that were at the early stages of apoptosis were labeled by Annexin V, whereas necrotic cells were labeled by propidium iodide, which permeated and stained their nuclei. Cells were incubated simultaneously with fluorescein isothiocyanate–labeled Annexin V and propidium iodide before quantification by FACS analysis.

Cell cycle assay

For cell cycle analysis, we used the 5-bromo-2′-deoxyuridine (BrdUrd) Flow kit purchased from BD PharMingen, according to the manufacturer's instructions. A20 cells were grown in six-well plates and treated with rR9-control (rR9-LACK) or rR9-GRIM19 for 24 hours. A total of 10 μL of BrdUrd solution (1 mmol/L BrdUrd in 1× PBS) was added to each well for 45 minutes at 37°C. The cells were fixed and permeabilized with Cytofix/Cytoperm buffer (BD PharMingen). Cellular DNA was denatured with DNase for 1 hour at 37°C. The cells were stained with anti-BrdUrd fluorescein isothiocyanate antibody and 7-aminoactinomycin D, and 100,000 events were analyzed by FACScan. Incorporated BrdUrd (with fluorescein isothiocyanate anti-BrdUrd) and total DNA content (with 7-aminoactinomycin D) were measured.

Tumor challenge study

In the tumor treatment study, A20 (1×10^6) cells were subcutaneously (s.c.) injected into BALB/c mice. EG.7 cells (1×10^6) and B16 cells (3×10^5) were also s.c. injected into C57BL/6 mice on day 0. Intratumoral (i.t.) injections of R9-fusion proteins (100 μg/100 μL/mouse) were done on days 9, 10, and 11. Tumor sizes were determined biweekly in a blinded fashion. Tumor index (in millimeters) = square root (length × width).

Cytotoxic T lymphocyte assay

On day 0, A20 (1×10^6) cells were s.c. injected into BALB/c mice. On days 9, 10, and 11, the mice were given

Published OnlineFirst August 3, 2010; DOI: 10.1158/1535-7163.MCT-09-1147

i.t. injections of the rR9-fusion proteins. On day 28, lymph node and spleen cells (pooled from two mice in each group) were harvested and restimulated *in vitro* with mitomycin C–treated (50 mg/mL for 45 minutes) A20 cells for 5 days. On day 33, cytotoxic T lymphocyte (CTL) activity was assessed using calcein release assays done as previously described (21, 22). Nonadherent spleen and lymph node cells were harvested from *in vitro* restimulation cultures and used as effector cells. A20 cells were labeled with calcein (Molecular Probes), washed, and added to 96-well round-bottomed microtiter plates with various numbers of effector cells. Plates were incubated for 3 hours, supernatants were recovered, and calcein release was measured using a Powerscan HT multidetection microplate reader (Dainippon Pharmaceutical Co.). The formula for percent-specific lysis is [(experimental – spontaneous)/(maximal – spontaneous)] × 100. Maximal lysis was achieved with 0.1% Triton X-100.

Histopathologic analysis

A20 cells (1×10^6) were injected s.c. into naïve mice on day 0. rR9-GRIM19 or rR9-control proteins were injected i.t. on day 9. Skin biopsies were done after 48 hours (day 11), and formaldehyde-fixed skin sections were stained with hematoxylin and eosin.

Statistical analysis

Results are expressed as mean ± SD. The differences between the means of the experimental groups were analyzed using Student's *t* test or ANOVA analyses. *P* values less than 0.01 or 0.05 were considered to be statistically significant (**, $P < 0.01$; *, $P < 0.05$).

Results

rR9-PTD–containing fusion proteins were delivered efficiently into cells

We previously reported that rR9-PTD–containing fusion proteins could be transduced into bone-marrow–derived dendritic cells in culture (21, 22). Subsequently, we investigated the efficiency of R9-fusion proteins in several murine cell lines (NIH3T3, fibroblasts; A20, B-cell lymphoma; B16, melanoma; and EG.7, thymoma cells) in culture, using rGFP proteins. As shown in Supplementary Fig. S1, the R9-PTD–containing GFP fusion protein (rR9-HA-GFP; 600 nmol/L) was more efficiently transduced into the cytoplasm of live cells (~100%) within 6 hours than rHA-GFP (non-R9). These results indicate that rR9-fusion proteins can be efficiently transduced into any type of cell in culture. To express the protein of interest, we have generated several rR9-PTD–containing fusion proteins, including rR9-OVA, rR9-mFCRL, rR9-Smad3 dominant-negative form (21–24), rR9-LACK, and rR9-GRIM19. SDS-PAGE characterization of the purified rR9-GRIM19 or rR9-control proteins (rR9-LACK, rR9-GFP, rR9-mFCRL) showed them to be predominantly a single species of the appropriate size (Fig. 1A). To assess the transduction efficiency of rR9-GRIM19, NIH3T3, A20, B16, and EG.7, cells were incubated in culture with rR9-GRIM19, washed, fixed, permeabilized, and stained with the anti-HA antibody. rR9-GRIM19 was distributed diffusely in the cytoplasm (Fig. 1B). Thus, like other rR9-fusion proteins, rR9-GRIM19 was also efficiently transduced into any cell.

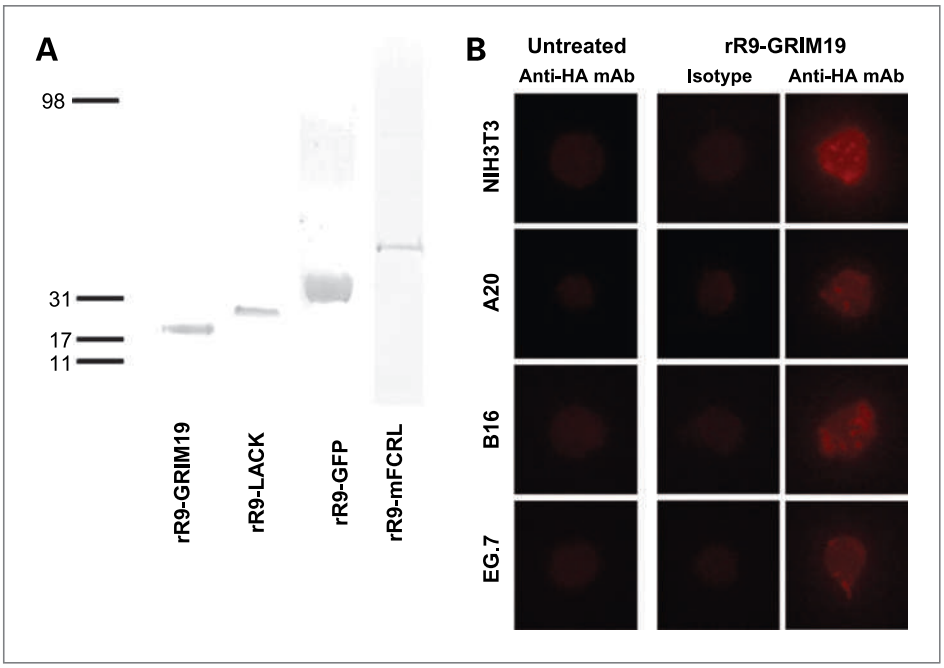

Figure 1. R9-PTD–containing fusion proteins and distribution of rR9-GRIM19 in culture. A, Coomassie blue–stained 4% to 12% SDS-PAGE gels resolving Ni-affinity– and ion exchange chromatography–purified fusion proteins. rR9-GRIM19 (20 kDa), rR9-LACK (a highly immunogenic foreign antigen in *Leishmania major*; 25 kDa), rR9-GFP (30 kDa), and rR9-mFCRL (reported as TAA; 46 kDa) constructs were generated as previously described (21–23). B, distribution of rR9-GRIM19 in cultured NIH3T3, A20, B16, and EG.7 cells. Cells were incubated with rR9-GRIM19 for 6 h, washed, fixed, permeabilized, and stained with anti-HA monoclonal antibody (mAb) or isotype IgG as a primary antibody and Cy-3–conjugated anti-mouse IgG as a secondary antibody. Images were captured by immunofluorescence microscopy. Data are representative of three individual experiments.

Published OnlineFirst August 3, 2010; DOI: 10.1158/1535-7163.MCT-09-1147

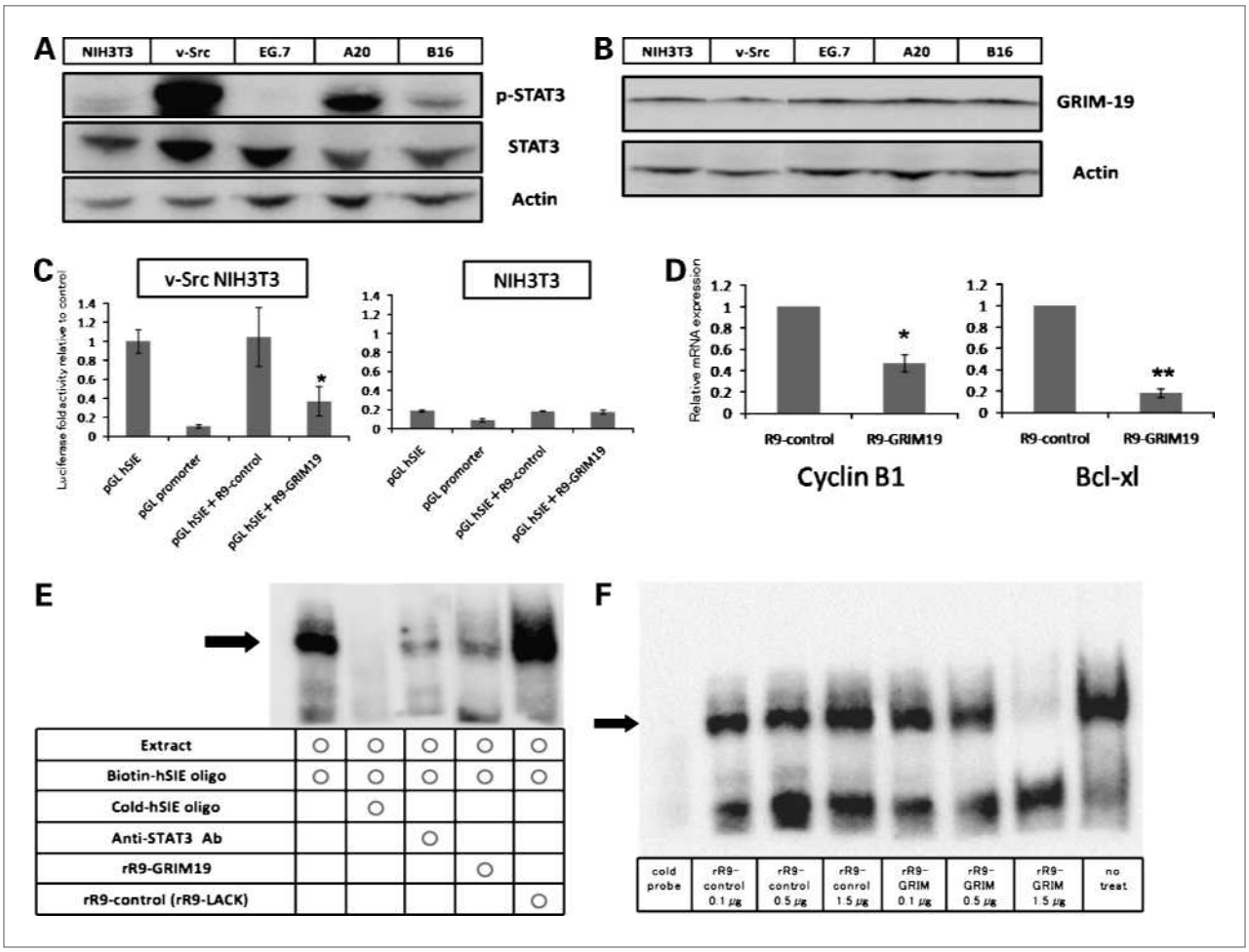

Figure 2. rR9-GRIM19 suppresses STAT3-mediated transcription. pSTAT3, STAT3, and actin (A), and GRIM-19 (B) expression in several tumor cell lines. Cell lysates from untreated NIH3T3, v-Src NIH3T3, EG.7, A20, and B16 cells were separated by SDS-PAGE and immunoblotted with the indicated antibodies as described in Materials and Methods. Data are representative of two individual experiments. C, effects of rR9-GRIM-19 on STAT3-dependent gene expression with luciferase reporter assay. v-Src NIH3T3 and parental NIH3T3 cells were transfected with luciferase reporter plasmids; 24 h later, cells were treated with rR9-GRIM19 or rR9-control. pGL hSIE (4× hSIE-pGL3-promoter plasmids) contains a STAT3-binding enhancer sequence upstream of the cytomegalovirus promoter site. The pGL promoter (pGL3-promoter plasmid) does not contain any enhancers. Transfections were done in triplicate, and results are presented as a fold change ± SD of firefly/Renilla. Data are representative of three independent experiments (*, $P < 0.05$). D, effect of rR9-GRIM-19 on STAT3-dependent gene expression. Real-time PCR with gene-specific primers was used for quantification of gene expression. mRNA was purified from v-Src NIH3T3 cells treated with rR9-GRIM19 or rR9-control. Relative mRNA expression levels were determined in triplicate by differences in cycle threshold numbers. Data are representative of two independent experiments (**, $P < 0.01$; *, $P < 0.05$). E, rR9-GRIM19 inhibits STAT3-hSIE interactions *in vitro* (EMSA). Nuclear extracts from v-Src NIH3T3 were incubated with the biotin-labeled hSIE probe for 20 min at room temperature. The binding was hampered by the 20-fold excess unlabeled hSIE (cold) probe, anti-STAT3 antibody, and rR9-fusion proteins. These samples were incubated for 20 min after incubating the nuclear proteins with the biotin-labeled probe. Data are representative of two independent experiments. F, rR9-GRIM19–mediated inhibitory effects on STAT3-hSIE complexes were dose dependent. rR9-fusion proteins (0.1, 0.5, and 1.5 μg) were incubated for 20 min after incubation of the nuclear proteins with the biotin probe. Data are representative of two independent experiments.

Expression of phosphorylated STAT3 and intrinsic GRIM-19 in cancer cells

Constitutive activation of STAT3 has been observed in many tumors. Subsequently, we evaluated STAT3 activity in several cancer cells by Western blotting analysis. We used v-Src cDNA-transfected NIH3T3 cells (v-Src NIH3T3) in which STAT3 was activated as a positive control. As shown in Fig. 2A, phosphorylated STAT3 (pSTAT3) was detected in A20 and B16 cells, but not in EG.7 or NIH3T3 cells. pSTAT3 was also detected in interleukin-6–stimulated NIH3T3 cells (Supplementary Fig. S2). We also evaluated GRIM-19 expression levels in these cells and found no significant differences between them (Fig. 2B).

rR9-GRIM19 suppresses STAT3-mediated transcription

It has been reported that the overexpression of GRIM-19 brought about by transfecting cDNA in cancer cells induced the inhibition of STAT3-dependent transcription

Published OnlineFirst August 3, 2010; DOI: 10.1158/1535-7163.MCT-09-1147

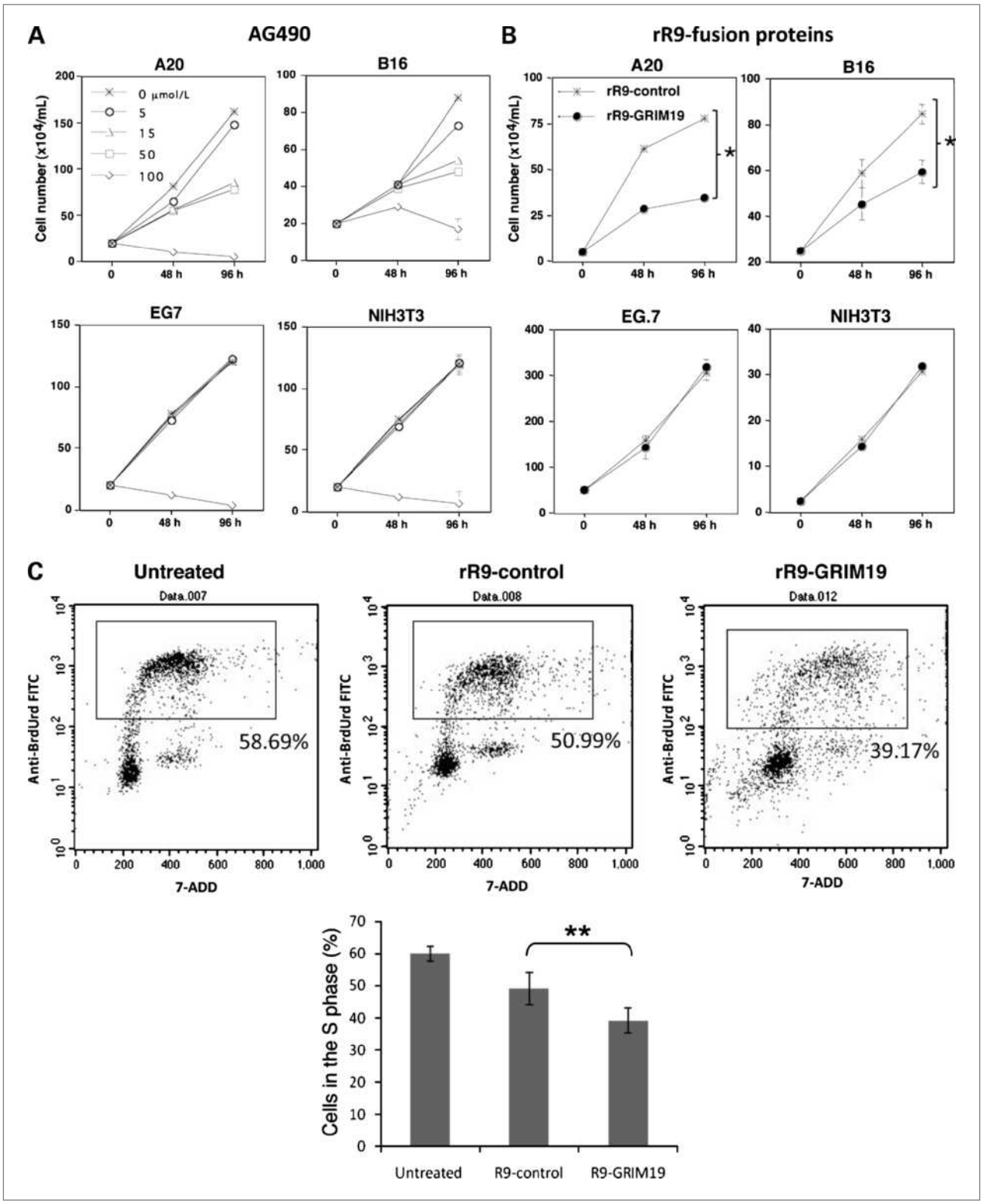

Figure 3. rR9-GRIM19 inhibits cell growth in STAT3-activated tumor cells in culture. A and B, AG490-/rR9-GRIM19–mediated inhibition of cell growth in culture. Cells were plated in six-well plates in triplicate in the presence of AG490 or rR9-fusion proteins [600 (nmol/L)/well]. Cell number was counted at 48 and 96 h. Data are representative of three individual experiments (*, $P < 0.05$). IC_{50} of AG490 was 8.5 (μmol/L)/mL. C, effect of rR9-GRIM19 on cell cycle analysis. Cell cycle analysis using BrdUrd and 7-aminoactinomycin D (7-AAD) was done as described in Materials and Methods. A20 cells in the S phase are shown as a square region. Data are representative of two individual experiments (**, $P < 0.01$). FITC, fluorescein isothiocyanate.

Published OnlineFirst August 3, 2010; DOI: 10.1158/1535-7163.MCT-09-1147

(11, 15, 18, 19). To assess whether the rR9-GRIM19 fusion protein could also inhibit the STAT3-dependent transcription, we performed a luciferase assay using v-Src NIH3T3 and parental NIH3T3 cells. We generated luciferase plasmids containing the STAT3-binding enhancer sequence (hSIE) upstream of the cytomegalovirus promoter site (pGL hSIE), and compared them with the parental plasmid (pGL promoter). As shown in Fig. 2C, rR9-GRIM19–treated cells reduced STAT3-mediated luciferase transcription in v-Src NIH3T3 cells, but not in parental NIH3T3 cells. These effects were not observed in cells containing rR9-control protein (rR9-LACK). Subsequently, we confirmed that the expression of downstream molecules of STAT3 were significantly suppressed by rR9-GRIM19 in v-Src NIH3T3 using quantitative reverse transcriptase-PCR (Fig. 2D) and Western blotting analyses (Supplementary Fig. S2A). We also confirmed that rR9-GRIM19 could suppress downstream molecules of STAT3 in NIH3T3 cells stimulated with interleukin-6 (Supplementary Fig. S2C). These results indicate that overexpression of rR9-GRIM19 suppresses STAT3-mediated transcription.

It has been reported that GRIM-19 directly binds to STAT3 and inhibits STAT3-dependent transcription (17, 18). We performed EMSA to confirm that rR9-GRIM19 can interact physically with STAT3-hSIE complexes, incubating v-Src NIH3T3 nuclear extract with biotin-labeled hSIE double-stranded oligos as a probe. We identified

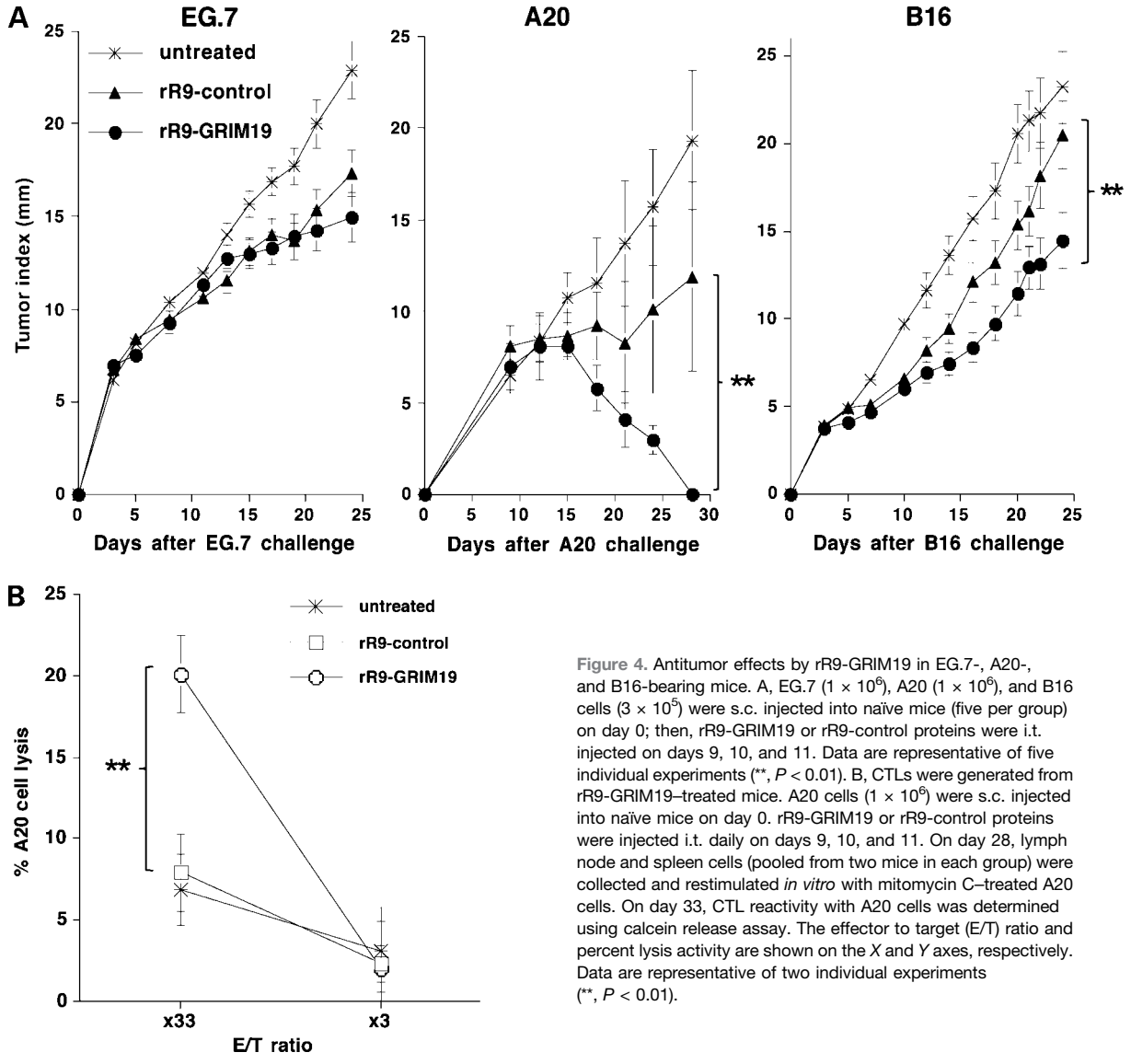

Figure 4. Antitumor effects by rR9-GRIM19 in EG.7-, A20-, and B16-bearing mice. A, EG.7 (1×10^6), A20 (1×10^6), and B16 cells (3×10^5) were s.c. injected into naïve mice (five per group) on day 0; then, rR9-GRIM19 or rR9-control proteins were i.t. injected on days 9, 10, and 11. Data are representative of five individual experiments (**, $P < 0.01$). B, CTLs were generated from rR9-GRIM19–treated mice. A20 cells (1×10^6) were s.c. injected into naïve mice on day 0. rR9-GRIM19 or rR9-control proteins were injected i.t. daily on days 9, 10, and 11. On day 28, lymph node and spleen cells (pooled from two mice in each group) were collected and restimulated *in vitro* with mitomycin C–treated A20 cells. On day 33, CTL reactivity with A20 cells was determined using calcein release assay. The effector to target (E/T) ratio and percent lysis activity are shown on the *X* and *Y* axes, respectively. Data are representative of two individual experiments (**, $P < 0.01$).

Published OnlineFirst August 3, 2010; DOI: 10.1158/1535-7163.MCT-09-1147

STAT3-hSIE complexes by incubation with the excess unlabeled (cold) hSIE probe or STAT3-specific antibody (Fig. 2E). Coincubation with rR9-GRIM19 diminished this band. Moreover, rR9-GRIM19–mediated inhibitory effects on STAT3-hSIE complexes were dose dependent (Fig. 2F). In contrast, such inhibitory effects were not observed in rR9-control (rR9-LACK) protein. We also confirmed that rR9-GRIM19 can directly interact with STAT3 *in vitro* by pull-down analyses (Supplementary Fig. S3). These results indicate that rR9-GRIM19 can functionally interact with STAT3 complexes and block DNA binding in a dose-dependent manner.

rR9-GRIM19 inhibits cell growth in STAT3-activated tumor cells

STAT3 participates in the regulation of key processes of malignant progression, including tumor proliferation, antiapoptosis, and tumor angiogenesis (7). Thus, we next investigated the antitumor effects of rR9-GRIM19 in cancer cells. As shown in Fig. 2A, pSTAT3 was highly expressed in A20 cells, moderately in B16 cells, and marginally in EG.7 and NIH3T3 cells. Using these cell lines, we investigated whether rR9-GRIM19 inhibits cell growth in culture by comparing these effects with those of the Jak2/gp130 (STAT3) inhibitor AG490. As shown in Fig. 3A and B, STAT3 inhibitors suppressed the growth of A20 and B16 cells, but not EG.7 or NIH3T3 cells. These effects correlated with the expression levels of pSTAT3. In addition, to evaluate the cell death pathway, we then performed a propidium iodide–Annexin assay using A20 and EG.7 cells treated with PBS, rR9-control (rR9-LACK), rR9-GRIM19, and AG490. Annexin V–positive cells increased in A20 cells with rR9-GRIM19 treatment, but not in EG.7 cells (Supplementary Fig. S4B). We next confirmed the expression of downstream molecules of STAT3 by quantitative reverse transcriptase-PCR and found that rR9-GRIM19 significantly suppressed the expression of cyclin B1 and Bcl-xl in B16 and A20 cells, but not in EG.7 cells (Supplementary Fig. S4A). Furthermore, rR9-GRIM19 was able to induce cell cycle (G_1) arrest in A20 cells (Fig. 3C). These results indicate that rR9-GRIM19 can induce the inhibition of cell growth by inducing G_1 arrest and cell death in tumor cells expressing pSTAT3. In contrast, these effects were not observed in tumor cells with low or no STAT3 activity.

Treatment effects with rR9-GRIM19 in tumor-bearing mice

We have previously reported that intradermal (i.d.) or i.t. injections of rR9-fusion proteins remained at the injection area for a long time. rR9-fusion proteins were efficiently transduced into the cytoplasm of locally injected tissues in mice (23). First, we evaluated the cytotoxicity of rR9-GRIM19 and pharmacologic STAT3 inhibitors by i.d. injections in naïve mice. Histopathologic analysis showed neutrophilic, lymphocytic, and monocytic infiltration in the skin injected with rR9-GRIM19 (Supplementary Fig. S5). In contrast, epidermal necrosis and dermal infiltration of inflammatory cells were observed in the area injected with AG490 or JSI-124. Therefore, i.d. injections of rR9-GRIM19 did not induce local and systemic effects to a greater extent in naïve mice than with AG490 or JSI-124. Subsequently, we investigated the antitumor effects by i.t. injections of rR9-fusion proteins *in vivo*. On day 0, tumor cells were inoculated, then rR9-GRIM19 or rR9-control proteins were injected i.t. on days 9, 10, and 11. I.t. injection of rR9-GRIM19 significantly reduced the growth of A20 and B16, but not EG.7, cells (Fig. 4A). Surprisingly, rR9-GRIM19 completely suppressed tumor growth in A20-bearing mice. Treatment results for A20 cells are summarized in Fig. 5. We have recently reported that i.t. injections of the highly immunogenic rR9-protein antigens elicited Ag-specific immune responses and strong antitumor effects with OVA as a tumor vaccination model (23). Moreover, we found that mFCRLA is the tumor-associated autoantigen (TAA) of A20 B-cell lymphoma cells (21). Although i.t. injections of not only rR9-mFCRL but also rR9-GRIM19 induced antitumor effects, the antitumor potency of rR9-GRIM19 was greater than that of rR9-mFCRL (Fig. 5). We also performed an A20 rechallenge study. Mice that had rejected an A20 tumor once were rechallenged on day 60 with A20 cells, and all mice that had rejected A20 also rejected the rechallenged A20 cells (data not shown). Mice that had (twice) rejected A20 remained healthy after 6 months. In addition, we performed a CTL assay using untreated rR9-control (rR9-GFP) and rR9-GRIM19–treated mice. As shown in Fig. 4B, A20-specific CTLs were generated in rR9-GRIM19–treated mice.

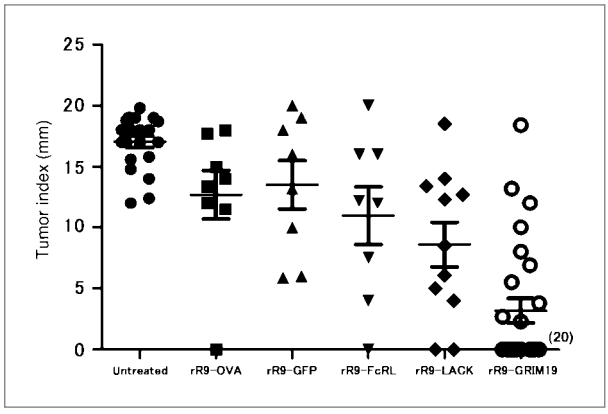

Figure 5. Summary of antitumor effects after treatment with R9-fusion proteins. Data from six individual treatment studies in A20-bearing mice (using the same protocol as described in Fig. 4A) were pooled (days 22–24 data reported). Individual tumor burdens represent the tumor indices (square root of the product of horizontal and vertical dimensions) in millimeters. Average tumor indices ± SD were also indicated. A one-way ANOVA test was done, finding a significant difference in tumor index among rR9-fusion protein treatment group (rR9-GRIM19 versus others; $P < 0.001$).

Published OnlineFirst August 3, 2010; DOI: 10.1158/1535-7163.MCT-09-1147

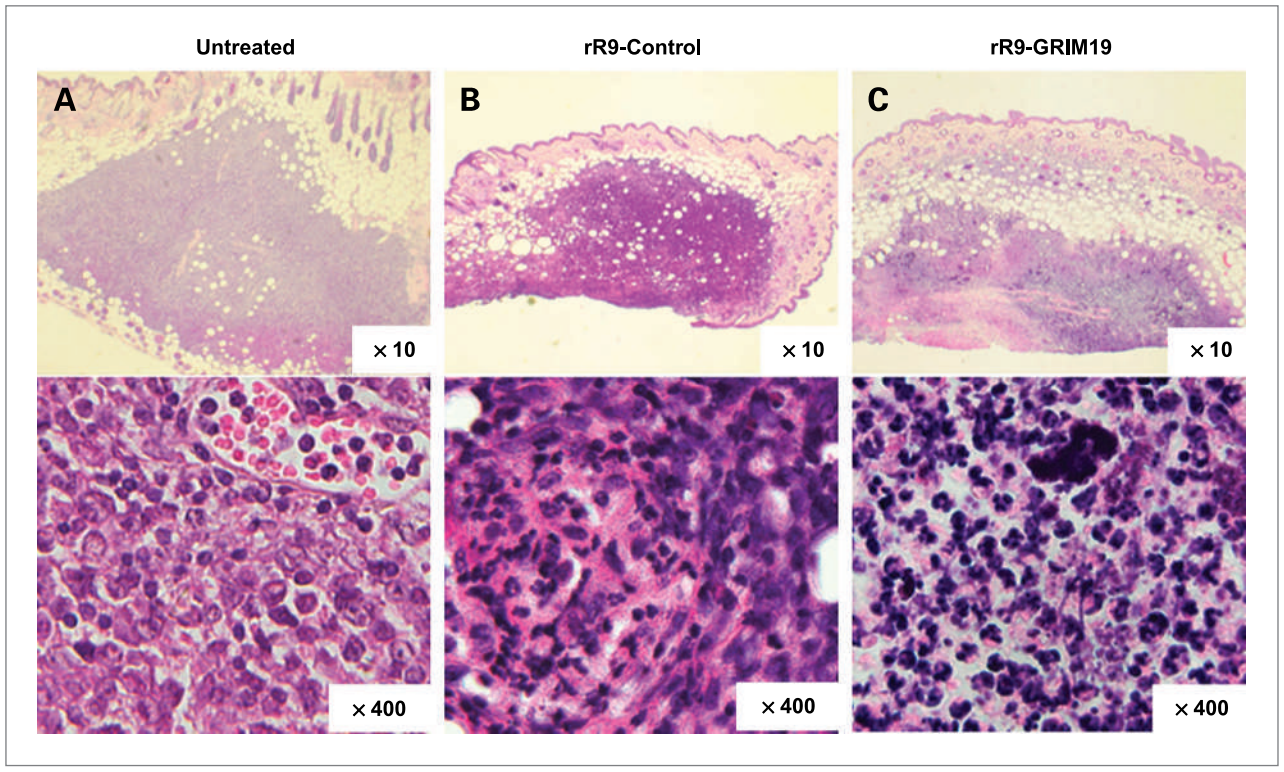

Figure 6. Histopathologic analyses at the tumor sections in A20-bearing mice. A to C, A20 cells (1×10^6) were injected s.c. into naïve mice on day 0. rR9-GRIM19 or rR9-control proteins were injected i.t. on day 9. Skin biopsies were done after 48 h (day 11), and vertical skin sections were stained with hematoxylin and eosin (A, untreated; B, rR9-GFP as control; C, rR9-GRIM19). Data are representative of two individual experiments (**, $P < 0.01$).

These results indicate that i.t. injections of rR9-GRIM19 stimulates antitumor immunity against A20 cells. Moreover, histopathologic analyses were done 48 hours after i.t. injections of rR9-GRIM19 or the rR9-control protein (rR9-GFP) on day 9 in A20 tumor–bearing mice (Fig. 6). Aggregation, degeneration of nucleus, and severe infiltration of inflammatory cells (mainly neutrophils) were observed after rR9-GRIM19 injection. In contrast, marginal infiltration of inflammatory cells was observed after rR9-control (rR9-GFP) injection.

Discussion

Recent studies in animal models using a dominant-negative form of STAT3 and a constitutively active mutant of STAT3, as well as the prevalence of constitutively activated STAT3 in many human cancers, strongly suggest that STAT3 has a causal role in oncogenesis (29–31). Also, there have been reports that immunosuppressive microenvironments are elicited by the constitutive activation of STAT3 in cancer and stromal cells, including melanoma (5–7). Currently, several immunotherapeutic approaches have been applied in melanoma-bearing hosts to induce/enhance melanoma-specific CTL activities in humans as well as in murine models using TAA. However, few strategies have accomplished antitumor effects in treatment studies. Our initial purpose was to establish safe and appropriate methods to inhibit the STAT3-mediated signal transduction in the cancer microenvironment. Our preliminary experiments show that pharmacologic STAT3 inhibitors induce severe local side effects such as skin ulcers when applied i.d., even in naïve mice (Supplementary Fig. S5). Our present data also show that these STAT3 inhibitors elicit unwanted cytotoxic effects in higher concentrations in any cell in culture (Fig. 3A). Previously, we have proposed that *in vivo* application of R9-PTD–containing fusion proteins to the local skin lesions/tumor mass might be useful as a novel cell transduction approach (23). Recently, we have investigated the immunogenicity of rR9-PTD–containing fusion proteins by i.t. injections in cancer-bearing mice. Our preliminary data showed that strong inflammatory immune responses with antitumor effects were elicited by rR9-containing immunogenic foreign Ags (rR9-OVA, rR9-LACK), but not by rR9-containing less-immunogenic Ags (rR9-GFP) nor rR9-containing TAA (rR9-mFCRL).[1] In contrast to the immunogenic foreign Ags or cancer-specific TAA, most types of cells express (native) GRIM-19, and only minimal local infiltration of inflammatory cells was

[1] Manuscript in submission.

Published OnlineFirst August 3, 2010; DOI: 10.1158/1535-7163.MCT-09-1147

observed in the injection area of naïve mice by rR9-GRIM19 (Supplementary Fig. S5). Therefore, the local application of rR9-GRIM19 as a novel STAT3 inhibitor might have some advantages for molecular-targeting therapy without major systemic/local side effects.

Although i.t. injections of rR9-GRIM19 in B16-bearing mice elicited antitumor effects, these effects were more significant in A20-bearing mice. Interestingly, these antitumor effects were higher than those observed in i.t. injections of rR9-mFCRL (TAA to A20 cells) or rR9-GFP (Fig. 5). We also showed that mice that had rejected A20 cells through i.t. injections of rR9-GRIM19 also rejected A20 cells with acquisition of A20-specific CTL activities (Fig. 4B). However, our preliminary data showed that peritumoral injections or i.d. injections away from tumor site of rR9-GRIM19 to A20-bearing mice showed little antitumor effects (data not shown). Thus, all these data indicate that i.t. injections of rR9-GRIM19 are critical for the induction of strong antitumor effects by inhibiting STAT3-mediated oncogenetic pathways, including derepression of immune responses to cancer cells. We are currently investigating the mechanism of antitumor effects by rR9-GRIM19 as a novel immunologic modifier, as well as the enhanced antitumor effects combined with cancer immunotherapies with TAA and/or adjuvants.

Recently, there have been several reports that STAT3 is also involved in cellular respiration and Ras-dependent oncogenic transformation through the mitochondrion, independent from transcriptional activities (32, 33). We are also investigating whether mitochondrial function is modulated in rR9-GRIM19–transduced cancer cells.

Disclosure of Potential Conflicts of Interest

No potential conflicts of interest were disclosed.

Grant Support

Ministry of Education and Science of the Japanese Government (grant no. 20390306, 18591241).

The costs of publication of this article were defrayed in part by the payment of page charges. This article must therefore be hereby marked *advertisement* in accordance with 18 U.S.C. Section 1734 solely to indicate this fact.

Received 01/04/2010; revised 05/19/2010; accepted 06/11/2010; published OnlineFirst 08/03/2010.

References

1. Bromberg JF, Wrzeszczynska MH, Devgan G, et al. Stat3 as an oncogene. Cell 1999;98:295–303.
2. Yu CL, Meyer DJ, Campbell GS, et al. Enhanced DNA-binding activity of a Stat3-related protein in cells transformed by the Src oncoprotein. Science 1995;269:81–3.
3. Bromberg JF, Horvath CM, Besser D, Lathem WW, Darnell JE, Jr. Stat3 activation is required for cellular transformation by v-src. Mol Cell Biol 1998;18:2553–8.
4. Yu H, Jove R. The STATs of cancer—new molecular targets come of age. Nat Rev Cancer 2004;4:97–105.
5. Wang T, Niu G, Kortylewski M, et al. Regulation of the innate and adaptive immune responses by Stat-3 signaling in tumor cells. Nat Med 2004;10:48–54.
6. Gamero AM, Young HA, Wiltrout RH. Inactivation of Stat3 in tumor cells: releasing a brake on immune responses against cancer? Cancer Cell 2004;5:111–2.
7. Yu H, Kortylewski M, Pardoll D. Crosstalk between cancer and immune cells: role of STAT3 in the tumour microenvironment. Nat Rev Immunol 2007;7:41–51.
8. Niu G, Shain KH, Huang M, et al. Overexpression of a dominant-negative signal transducer and activator of transcription 3 variant in tumor cells leads to production of soluble factors that induce apoptosis and cell cycle arrest. Cancer Res 2001;61:3276–80.
9. Niu G, Heller R, Catlett-Falcone R, et al. Gene therapy with dominant-negative Stat3 suppresses growth of the murine melanoma B16 tumor *in vivo*. Cancer Res 1999;59:5059–63.
10. Leong PL, Andrews GA, Johnson DE, et al. Targeted inhibition of Stat3 with a decoy oligonucleotide abrogates head and neck cancer cell growth. Proc Natl Acad Sci U S A 2003;100:4138–43.
11. Zhang L, Gao L, Li Y, et al. Effects of plasmid-based Stat3-specific short hairpin RNA and GRIM-19 on PC-3M tumor cell growth. Clin Cancer Res 2008;14:559–68.
12. Angell JE, Lindner DJ, Shapiro PS, Hofmann ER, Kalvakolanu DV. Identification of GRIM-19, a novel cell death-regulatory gene induced by the interferon-β and retinoic acid combination, using a genetic approach. J Biol Chem 2000;275:33416–26.
13. Fearnley IM, Carroll J, Shannon RJ, et al. GRIM-19, a cell death regulatory gene product, is a subunit of bovine mitochondrial NADH:ubiquinone oxidoreductase (complex I). J Biol Chem 2001;276:38345–8.
14. Murray JG, Zhang B, Taylor SW, et al. The subunit composition of the human NADH dehydrogenase obtained by rapid one step immunopurification. J Biol Chem 2003;278:13619–22.
15. Huang G, Lu H, Hao A, et al. GRIM-19, a cell death regulatory protein, is essential for assembly and function of mitochondrial complex I. Mol Cell Biol 2004;24:8447–56.
16. Alchanati I, Nallar SC, Sun P, et al. A proteomic analysis reveals the loss of expression of the cell death regulatory gene GRIM-19 in human renal cell carcinomas. Oncogene 2006;25:7138–47.
17. Lufei C, Ma J, Huang G, et al. GRIM-19, a death-regulatory gene product, suppresses Stat3 activity via functional interaction. EMBO J 2003;22:1325–35.
18. Zhang J, Yang J, Roy SK, et al. The cell death regulator GRIM-19 is an inhibitor of signal transducer and activator of transcription 3. Proc Natl Acad Sci U S A 2003;100:9342–7.
19. Chidambaram NV, Angell JE, Ling W, Hofmann ER, Kalvakolanu DV. Chromosomal localization of human GRIM-19, a novel IFN-β and retinoic acid-activated regulator of cell death. J Interferon Cytokine Res 2000;20:661–5.
20. Kalakonda S, Nallar SC, Gong P, et al. Tumor suppressive protein gene associated with retinoid-interferon- induced mortality (GRIM)-19 inhibits src-induced oncogenic transformation at multiple levels. Am J Pathol 2007;171:1352–68.
21. Inozume T, Mitsui H, Okamoto T, et al. Dendritic cells transduced with autoantigen FCRLA induce cytotoxic lymphocytes and vaccinate against murine B-cell lymphoma. J Invest Dermatol 2007;127:2818–22.
22. Mitsui H, Inozume T, Kitamura R, Shibagaki N, Shimada S. Polyarginine-mediated protein delivery to dendritic cells presents antigen more efficiently onto MHC class I and class II and elicits superior antitumor immunity. J Invest Dermatol 2006;126:1804–12.
23. Mitsui H, Okamoto T, Kanzaki M, et al. Intradermal injections of

Published OnlineFirst August 3, 2010; DOI: 10.1158/1535-7163.MCT-09-1147

polyarginine- containing immunogenic antigens preferentially elicit Tc1 and Th1 activation and antitumor immunity. Br J Dermatol 2010;162:29–41.
24. Kanzaki M, Shibagaki N, Hatsushika K, et al. Human eosinophils have an intact Smad signaling pathway leading to a major transforming growth factor-β target gene expression. Int Arch Allergy Immunol 2007;142:309–17.
25. Kaplan IM, Wadia JS, Dowdy SF. Cationic TAT peptide transduction domain enters cells by macropinocytosis. J Control Release 2005; 102:247–53.
26. Fuchs SM, Raines RT. Pathway for polyarginine entry into mammalian cells. Biochemistry 2004;43:2438–44.
27. Cai S-R, Xu G, Becker-Hapak M, et al. The kinetics and tissue distribution of protein transduction in mice. Eur J Pharm Sci 2006;27:311–9.
28. Gurunathan S, Sacks DL, Brown DR, et al. Vaccination with DNA encoding the immunodominant LACK parasite antigen confers protective immunity to mice infected with *Leishmania major*. J Exp Med 1997;186:1137–47.
29. Bowman T, Yu H, Sebti S, et al. Signal transducer and activators of transcription: novel targets for anticancer therapeutics. Cancer Conrol 1999;6:427–35.
30. Turkson J, Jove R. STAT proteins: novel molecular targets for cancer drug discovery. Oncogene 2000;19:6613–26.
31. Bowman T, Garcia R, Turkson J, et al. STATs in oncogenesis. Oncogene 2000;19:2474–88.
32. Wegrzyn J, Potla R, Chwae YJ, et al. Function of mitochondrial Stat3 in cellular respiration. Science 2009;323:793–7.
33. Gough DJ, Corlett A, Schlessinger K, et al. Mitochondrial STAT3 supports Ras-dependent oncogenic transformation. Science 2009; 324:1713–6.

AACR American Association for Cancer Research

Molecular Cancer Therapeutics

Overexpression of GRIM-19 in Cancer Cells Suppresses STAT3-Mediated Signal Transduction and Cancer Growth

Takashi Okamoto, Takashi Inozume, Hiroshi Mitsui, et al.

Mol Cancer Ther 2010;9:2333-2343. Published OnlineFirst August 3, 2010.